Can one hear structures of smectic films?

I. Kraus,* Ch. Bahr,† I. V. Chikina,‡ and P. Pieranski
Laboratoire de Physique des Solides, Université Paris–Sud, Bâtiment 510, 91405 Orsay, France
(Received 6 February 1998)

Drumhead vibrations are used to detect phase transitions in smectic films. We point out experimentally and theoretically that vibrational eigenmodes are specially sensitive to structural transitions when the films are curved. In particular, stacking transitions in thick SmB_{cryst}-like films of 7O.7 are detected.
[S1063-651X(98)08907-7]

PACS number(s): 61.30.−v, 64.70.Md

I. CAN ONE HEAR STRUCTURES OF SMECTIC FILMS?

The question addressed in the title of this paper is a paraphrase of the celebrated article ''Can one hear the shape of a drum?'' [1] in which the author, Mark Kac, asked, a long time ago, whether one can recognize the shape of a drum from its sound.

The drum considered by Kac consists of a thin, perfectly flexible, elastic, and isotropic membrane, spanned on a flat boundary Γ (Fig. 1). When the two-dimensional density of the membrane ρ is uniform, and the tension τ to which the membrane is submitted is isotropic and uniform as well, the drum's vertical displacement $\zeta(x,y;t)$ in the limit of small amplitudes obeys the wave equation

$$\frac{\partial^2\zeta}{\partial t^2}=\frac{\tau}{\rho}\left(\frac{\partial^2\zeta}{\partial x^2}+\frac{\partial^2\zeta}{\partial y^2}\right), \tag{1.1}$$

with the boundary conditions

$$\zeta(\Gamma;t)=0. \tag{1.2}$$

Such a drum is able to produce pure tones of frequency ω_n which are known as normal modes and have the form

$$\zeta_n(x,y;t)=\zeta_n(x,y)e^{i\omega_n t}. \tag{1.3}$$

The frequency ω_n of the eigenmodes and their associated geometry $\zeta_n(x,y)$ satisfy the equation

$$\frac{\tau}{\rho}\left(\frac{\partial^2\zeta_n}{\partial x^2}+\frac{\partial^2\zeta_n}{\partial y^2}\right)+\omega_n^2\zeta_n=0, \tag{1.4}$$

which can be rewritten in a dimensionless form using L, the length scaling the size of the drum, as

$$\left(\frac{\partial^2\zeta_n}{\partial\tilde{x}^2}+\frac{\partial^2\zeta_n}{\partial\tilde{y}^2}\right)+\lambda_n\zeta_n=0, \tag{1.5}$$

where

$$\omega_n^2=\lambda_n\left(\frac{1}{L^2}\frac{\tau}{\rho}\right) \tag{1.6}$$

and

$$\tilde{x}=\frac{x}{L}\quad\text{and}\quad\tilde{y}=\frac{y}{L}. \tag{1.7}$$

From Kac's mathematical point of view, the answer to his question is given when the nature of the relationship between the shape Γ and the spectrum of eigenvalues λ_n is found. In particular, Kac wondered whether the spectrum λ_n is unique for every shape of the boundary. We know today that the answer to this last question is ''no,'' because there are known examples of different shapes having the same spectra of eigenvalues [2–5].

From the physical point of view represented in the present paper, the main interest in studying the sound of a drum is to extract information on the physical properties of the drum membrane from its λ_n spectrum. It has been shown previously [6,7] that the so-called free-standing smectic films in ''fluid'' phases such as SmA or SmC behave indeed, to high accuracy, as such ideal drums and are characterized by only two physical parameters: the two-dimensional (2D) density ρ and the isotropic tension τ. Indeed, unlike soap bubbles, which must be held in a wet atmosphere in order to preserve their stability, smectic films can vibrate in quasivacuum. When submitted to vacuum, they evaporate slightly, unless the vapor pressure of the liquid crystal material reaches its saturation value, which is by few orders of magnitude lower than the one of water. Thus the mass of the surrounding gas

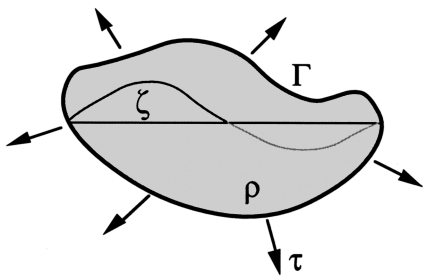

FIG. 1. Kac's drum: a perfectly flexible and homogeneous membrane of the density ρ, spanned on contour Γ and submitted to isotropic tension τ.

*Present address: Institut de Physique et Chimie des Matériaux, 23 rue du Loess, 67037 Strasbourg Cedex, France.
†Present address: University of Marbourg, Institute of Physical Chemistry, D-35032 Marbourg, Germany.
‡Present address: Institute of Microelectronic Technology of Russian Academy of Science, Chernogolovka, Russia.

put into motion by the vibrating film can be neglected with respect to the mass ρ of the film itself. It is also important to emphasize that in the liquidlike SmA or SmC phases, the restoring force is mainly due to the tension τ of the smectic film. This is so because the curvature elasticity effects of reasonably thin films can be neglected with respect to the tension effects. To sum up, in the case of smectic films in SmA or SmC phases, for known shape Γ and size L of the frame, the frequency of eigenmodes provides information on the ratio τ/ρ of the tension τ to the density ρ of the membrane in the case of smectic films in SmA or SmC phases, for known shape Γ and size L of the frame.

In the present paper we will show that smectic films in crystalline smectic phases (SmB, SmG, etc.) no longer behave as an ideal drum because their 3D elasticity contributes to the restoring force and affects the tune of the drum. Moreover, we will point out that the change of tune due to the 3D elasticity is very sensitive to the 3D shape of the drum membrane, that is to say, to the built-in Gaussian curvature of the film due to the deviation from the planar shape of the contour Γ. In other words, we will show that *one can hear both the structure and shape of the drum.*

The paper is organized as follows. In Sec. II the genesis, structure, and physical properties of smectic films are briefly discussed on the basis of the thermodynamic point of view previously developed in Ref. [7]. In Sec. III the equation of motion of smectic films is revisited in order to take into account effects due to the curvature at rest and to the 3D elasticity. Section IV is devoted to the description of the experimental setup developed for experiments involving curved smectic films vibrating in vacuum. Experimental results obtained mainly with films of 7O.7 are presented and discussed in the last sections.

II. THERMODYNAMICS OF SMECTIC FILMS

Before we start to discuss the effects of the Gaussian curvature on the vibrations of smectic films, it seems necessary to make a short introduction concerning the structure of smectic films, and to make clear that smectic films are very peculiar objects from the structural, thermodynamic, and mechanical points of view.

The most important fact about smectic films is that they cannot exist on their own, but must stay suspended on a stiff enough frame. This is so because the elastic moduli of smectic phases, even of those that are crystalline in three dimensions (SmB_{cryst} or SmG), are so low that they are unable to stand strains due to the surface tension, unlike thin slices of ordinary 3D crystals such as silicon. Being suspended, smectic films are always surrounded by a meniscus connecting them to the frame. It is possible only when the liquid crystal material has a tendency to wet the frame.

The limit between the film made of an arbitrary number N of molecular layers and the meniscus is well defined. Indeed, in its thinnest portion, the linear meniscus shown on Fig. 2 is nothing but a collection of monomolecular steps whose density per unit length $n(x)$ determines the shape of the meniscus $h(x)$,

$$h(x)=h_f+d\int n(x)dx, \tag{2.1}$$

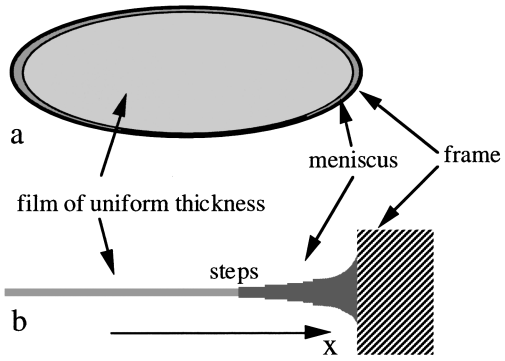

FIG. 2. Structure of a smectic film suspended on a circular frame: (a) Perspective view of the film. (b) Enlarged view of the meniscus (in sections) which, in the vicinity of the film, can be seen as a collection of steps pushed toward the frame.

where $h(x)$ is the local thickness, and d is the thickness of one molecular layer. The first step of the meniscus constitutes obviously the limit of the film [8]. The position of the first step as well as the whole distribution of other steps $n(x)$ in the meniscus are determined by forces acting on them [9]. The stability of the first step position requires that it must be submitted to a thermodynamic force pushing it toward the next steps of the meniscus which will exert a repulsive action on the first step and stabilize the edge of the meniscus. In the opposite case, that is to say, if the first step was pulled by the thermodynamic force toward the center of the film, its diameter would decrease and, finally, the step would collapse.

Starting from the discussion of the behavior of the first step in the meniscus, we arrived at a more general question about the sense and amplitude of the thermodynamic force acting on an isolated straight step separating two portions of the film with different thicknesses N and $N+1$. This force being nothing else but the difference between the tensions τ_N and τ_{N+1} of films of thicknesses N and $N+1$, we have to find how the film tension depends on the thickness.

From the thermodynamic point of view, the tension of smectic films is similar to the pressure p in 3D materials, and is defined as the derivative of the free energy per molecule $f_N(a,T)$ with respect to the surface area a per molecule (T refers to the temperature):

$$\tau_N=\frac{\partial f_N(a,T)}{\partial a}. \tag{2.2}$$

Let us emphasize that the free energy f_N as well as the surface area a occurring here are quantities averaged on the thickness of the film. In particular, the surface area per molecule is defined as the ratio

$$a=A/\mathcal{N} \tag{2.3}$$

of the film area to the total number of molecules $\mathcal{N}$ in it.

The value of the film tension τ_N is determined by the condition of its equilibrium with the meniscus which, in most cases, has a large volume and acts as a reservoir of particles fixing the chemical potential μ_{men} in the system. As shown in Fig. 3 the equilibrium condition

$$\mu_N=f_N(\alpha)-\tau_N a=\mu_{\text{men}} \tag{2.4}$$

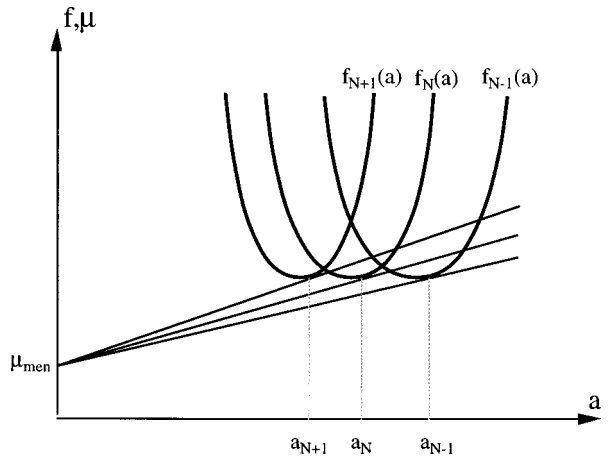

FIG. 3. Geometrical representation of the thermodynamic equilibrium between the meniscus fixing the chemical potential μ_{men} and films of thicknesses $N-1$, N, and $N+1$. The tension τ_N of the film of thickness N corresponds to the slope of the line starting from μ_{men} and tangent to the function $f_N(a)$.

leads to the construction of a tangent to the curve $f_N(a)$ intersecting the ordinate axis at μ_{men}. Clearly, the resulting slope τ_N depends on the position and shape of the function $f_N(a)$, which can be approximated as

$$f_N(a)=f_{N\,\min}+B_N(a-a_{N\,\min})^2+0(a^4). \tag{2.5}$$

In the simplest model, where the smectic film is treated as a stack of N identical layers, $f_{N\,\min}=f_0$ is independent of N, $a_{N\,\min}=\alpha/N$ and $B_N=\beta N$ with α and β constants. Within such a model, it results from the construction of Fig. 3 that the tension of the film increases with its thickness when $\mu_{\text{men}}<f_0$. In other words, for each N one has

$$\tau_N<\tau_{N+1}. \tag{2.6}$$

When this inequality holds, the collection of steps forming the meniscus is stable for any N, but the film itself is only metastable with respect to any decrease of its thickness [9]. In order to decrease the film thickness, a pore must be created in at least one of the N molecular layers forming the stack. This process is analogous to the nucleation of a new phase in the old one during a first-order phase transition. When the radius of the pore is large enough, that is to say larger than the critical radius r_c [7], the pore will open more and more until its edge hits the meniscus edge. In the opposite case, $r<r_c$, the pore will collapse. It is important to know that in most cases the nucleation barrier for the creation of a pore is much larger than kT, so that the metastability of smectic films with respect to the reduction of their thickness is only virtual. This explains the astonishing robustness of smectic films contrary to the proverbial fragility of soap bubbles.

The above analysis of the film stability has to be revisited when the structure of the N molecular layers depend on their position $i=1,\ldots,N$ in the stack or when the structure of the ith layer is a function of the total thickness of the stack. In such case, all coefficients of expression (2.5) can depend on N in a complex way. In particular it can happen that in some thickness interval $[N_1,N_2]$, the inequality is inverted:

$$\tau_N>\tau_{N+1}. \tag{2.7}$$

Thicknesses from the interval $[N_1,N_2]$ will thus be prohibited, and the meniscus will have a clifflike shape; the thickness of the film will jump from $N<N_1$ to $N>N_2$. As the free energy f_N depends on the temperature as well, such an interval of prohibited thicknesses can appear for some temperature range $[T_1,T_2]$. Outside $[T_1,T_2]$, a film of thickness $N_p[N_1,N_2]$ can coexist with a smooth meniscus. However, when the temperature enters the $[T_1,T_2]$ range, the $\Delta N=N_2-N_p$ steps of the meniscus will collapse until the film thickness reaches N_2.

It is obvious from the above considerations that the tension of smectic films is the parameter ruling their stability. From a formal point of view, the equilibrium states of a system in contact with a reservoir of particles are ruled by the grand canonical potential Ω which must be minimal. In our case, one has, by definition,

$$\Omega=F-\mu\mathcal{N} \tag{2.8}$$

where F is the total free energy, and $\mathcal{N}$ is the total number of molecules in the film. Using the definition of the chemical potential [Eq. (2.4)], one finds that

$$\Omega=\tau A, \tag{2.9}$$

where A is the total area of the film fixed by the frame. As expected, the tension of the film should be minimal for constant A.

In the above analysis of the thermodynamic equilibrium in smectic films, the free energy per molecule f_N, averaged over the film thickness, plays the central part. By definition, one has

$$f_N=\frac{1}{N}\sum_{i=1}^{N} f_{N_i} \tag{2.10}$$

where f_{N_i} stands for the free energy per molecule in the ith layer of the stack made of N layers. When the thickness of a smectic film is very small, the contribution to the average free energy $f_N(a)$ of molecular layers close to the film surfaces becomes important. In spite of exchanges of molecules from layer to layer, each of the layers in the stack can have a different structure in principle and, consequently, a different surface area or free energy per molecule. Indeed, interactions between layers and exchanges of molecules between adjacent layers impose only the equality of the chemical potential μ_{N_i}. The free energy f_{N_i} can be different provided the tension τ_{N_i}, defined separately for each of the layers, is properly adjusted. Obviously, because of different environments (because of the drastic change at the interfaces), structures in the surface layers can be very different from those in a bulk material at the same temperature. Moreover, these structures must depend on the film thickness N.

Because of the dependence of layers structure on the film thickness, the polymorphism of the smectic films can be different and sometimes richer than that of the bulk material. For this reason, the structural terminology coined for bulk smectic phases, where all layers are identical, cannot be used for smectic films such as it is. For example, in ALLO [10], in

the temperature range where the bulk material should be in the Sm*A* phase, films of thickness larger than 90 layers can have a hybrid structure: a Sm*A*-like core sandwiched between several Sm*C*-like surface layers. Such a structure can be described by the tilt angle distribution $\theta_i(T)$. In the limit of very large thicknesses, when the relative contribution of the surface layers to the averaged thermodynamic quantities can be neglected, one can say that the film structure is Sm*A*-like. Nevertheless, because of the presence of the Sm*C*-like layers, the symmetry of the whole film is broken and cannot be qualified as Sm*A*, strictly speaking. In the temperature range where the bulk material should be in the Sm*C* phase, the tilt angles $\theta_i(T)$ are larger than in the Sm*A*-like films. Thus the ''state'' of a smectic film can be established considering its tilt angle distribution $\theta_i(T)$. In ALLO films thicker than 90 layers, there is a discontinuous change in the tilt angle distribution as a function of the temperature. By continuity with the $N \Rightarrow \infty$ limit, such a structural change can be qualified as a Sm*A*-Sm*C*-like transition. For thicknesses less than 90 layers there is no discontinuity in the distribution $\theta_i(T)$ but just a continuous change: the Sm*A*-Sm*C* phase transition line in the (N,T) phase diagram terminates for $N=90$ at a critical point.

As a second example of the specific polymorphism of smectic films, important for the purpose of the present paper, let us quote that of $7O.7$ films established on the basis of the x-ray diffraction studies. On the (N,T) phase diagram established by Sirota *et al.* [11] the phase sequence in the $N \Rightarrow 8$ limit is

$$\text{C}/33\ ^\circ\text{C}/\text{Sm}G_{\text{cr}}/55\ ^\circ\text{C}/\text{Sm}B_{\text{cr}}/69\ ^\circ\text{C}/\text{Sm}C/72\ ^\circ\text{C}/\text{Sm}A/$$

$$83.7\ ^\circ\text{C}/\text{N}-84\ ^\circ\text{C}/\text{Iso},$$

but for thicknesses less than 10^3 Å, the Sm*F*-like structure appears between the Sm*B*-like and Sm*G*-like structures. The temperature range of the Sm*F*-like structure increases with decreasing N, mainly at the cost of the Sm*B*-like phase, with decreasing N. Another interesting feature of the $7O.7$ (N,T) phase diagram is the existence of stacking transitions between different variants of the Sm*B*-like phase, as pointed out in Refs. [11]. Our purpose here will be to show that all these structural transitions in $7O.7$ films can be detected ''by hearing the sound of the drum.''

III. MECHANICAL PROPERTIES OF SMECTIC FILMS

One can expect that vibrations of smectic films, when their structure is crystal-like, should be very sensitive to their shapes. Indeed, the common-day experience shows that the rigidity of an iron sheet depends a lot on its shape, and, consequently, quite complex shapes are generated in order to satisfy requirements for the rigidity.

In the case of smectic films, like for soap bubbles, the choice of shapes is limited to minimal surfaces. Indeed, surface strains that would result from any deviation of the minimal surface shape cannot be equilibrated by the bulk rigidity of smectic phases on a long time scale. This is quite similar to the necessity mentioned above of suspending smectic films on a rigid frame. More precisely, exchanges of molecules between smectic layers in the film and between the film and the meniscus are rapid enough to restore the minimal surface area of the film on a less-than-few-minutes time scale. Obviously, the relaxation time of such strains depends a lot on the structure of molecular layers in the films and on its thickness. It is of the order of 10^{-2} sec in thin films made of Sm*A*-like layers, but it can be as large as few minutes in thick films made of crystalline Sm*B*-like layers.

In conclusion, the drums we want ''to hear'' are all minimal surfaces and as such must have the zero mean curvature H. Using the expression of the mean curvature for surfaces of the Monge form $z=z(x,y)$, one obtains a nonlinear differential equation:

$$2H=\frac{1}{R_1}+\frac{1}{R_2}=\frac{(1+z_y^2)z_{xx}-2z_xz_yz_{xy}+(1+z_x^2)z_{yy}}{(1+z_x^2+z_y^2)^{3/2}}=0, \tag{3.1a}$$

where $1/R_1$ and $1/R_2$ are the principal curvatures of the surface, z_x and z_y are the first derivative of z with respect to x and y respectively, and z_{xx}, z_{xy}, and z_{yy} are second derivatives. Equation (3.1a) reduces to the linear Laplace equation

$$\frac{\partial^2 z}{\partial x^2}+\frac{\partial^2 z}{\partial y^2}=0 \tag{3.1b}$$

in the limit of almost flat shapes $z \approx 0$. The solutions of these differential equations depend on the shape Γ of the frame.

In the simplest case, invoked by Kac, the contour Γ is a flat curve and the smectic film is a plane. However, it is important to remark that such a perfectly flat film is only a mathematical concept because in practice several mechanisms will generate deviations from the flat shape. First of all, every smectic film is submitted to the gravity force which has to be equilibrated by the adequate deformation of the film. In the case when the film is horizontal and its surface density is given by $\rho_{\text{cl}}h$, one obtains

$$\tau\left(\frac{\partial^2 z}{\partial x^2}+\frac{\partial^2 z}{\partial y^2}\right)=\rho_{\text{cl}}hg, \tag{3.2}$$

where g is the gravity acceleration. On a circular contour of radius r_Γ, the film will take the shape of a paraboloid:

$$z(x,y)=\frac{r_\Gamma^2}{2R}-\frac{x^2+y^2}{2R}, \tag{3.3}$$

where the curvature radius R is inversely proportional to the film thickness N,

$$R=\frac{\tau}{\rho_{\text{cl}}hg}=\frac{R_1}{N}, \tag{3.4}$$

and where

$$R_1=\frac{\tau}{\rho_{\text{cl}}gd}=\frac{l^2}{d} \tag{3.5}$$

is the curvature radius calculated for one molecular layer of thickness d. In the above equation we introduce the capillary length 1 which for a film tension of the order of 50 dyn/cm and a density of $\rho_{\text{cl}}=1$ g/cm is of the order of 2 mm. The curvature radius R calculated for a two-layer films of the

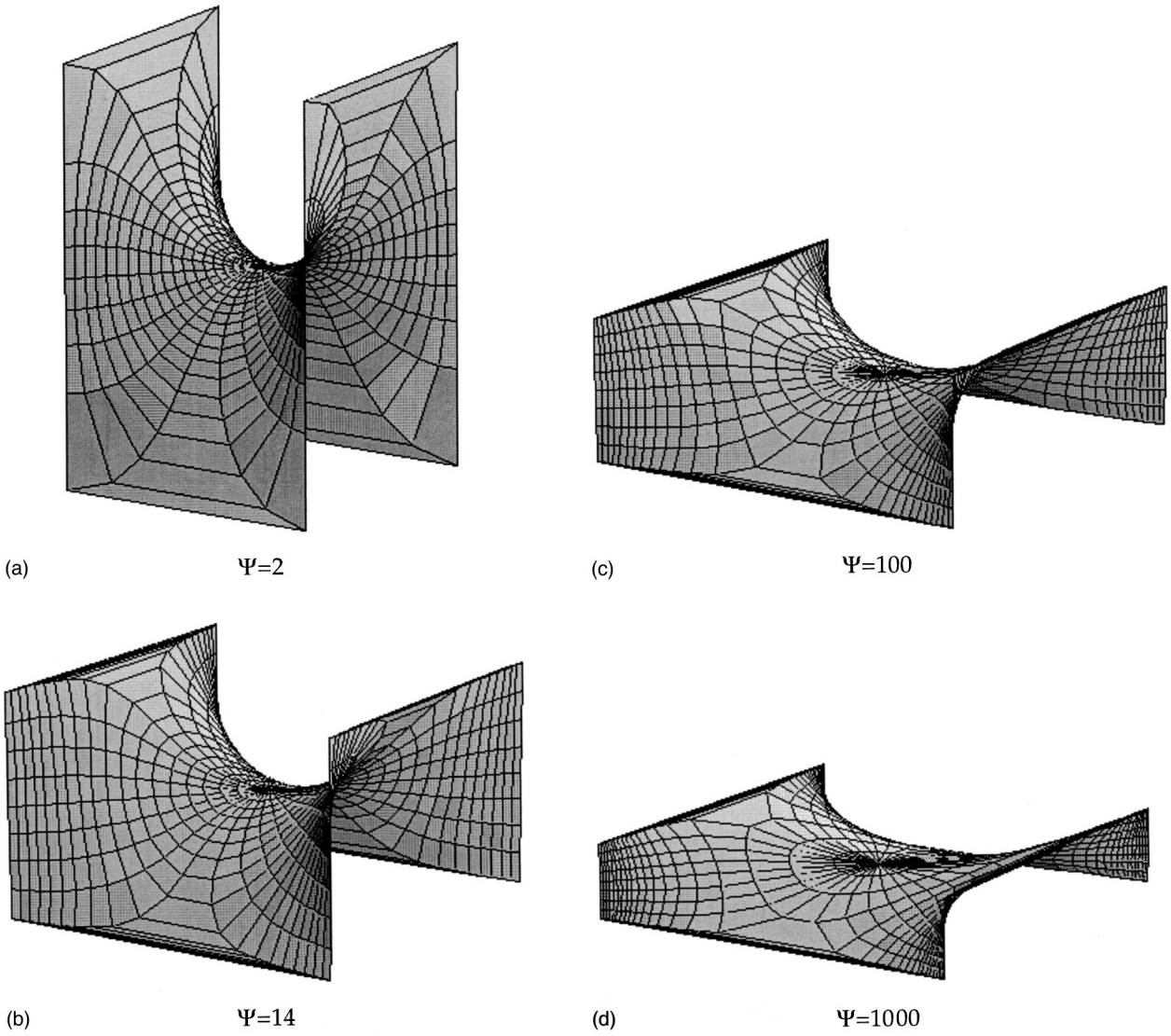

FIG. 4. Minimal surfaces spanned on a frame made of eight straight mutually orthogonal edges. These shapes are calculated by means of the Weierstrass' formulas [Eq. (3.7)] using the analytic function $R(z)=(z^8-\Psi z^4+1)^{-1/2}$. The aspect ratio $\alpha=L_z/L$ depends on the value of the parameter Ψ.

thickness $h=6\times10^{-7}$ cm is of the order of one kilometer, and seems enormous. However, the deflection in the center of the film of radius r_Γ,

$$z_{\max}=\frac{r_\Gamma^2}{2l^2}\,h, \tag{3.6}$$

is of the order of the film thickness for $r_\Gamma\approx1$ cm and thus, strictly speaking, cannot be neglected. The second source of deviation from the flat shape is due to the imperfections of the frame. For any frame constructed by conventional machining procedures, the scale of these imperfections is in the best case in the micrometer range. For the frames used in the present study and the previous studies, we estimate the imperfection to be in the 10^{-2}-cm range, that is to say, 10^3 times larger than the thickness $h=1000$ Å of a 30-layer film. Finally, as we shall see in Sec. IV, the film shape can be affected by a nonuniform distribution of the excess liquid crystal material in the meniscus. Without annealing the sample slightly below the SmA–nematic transition temperature, smectic films show corrugations located in the vicinity of the meniscus. Well visible in a reflecting microscope, the local curvatures of such corrugations can be fairly large, of the order of a few cm^{-1}. In conclusion, perfectly flat films do not exist in practice and one has to examine how local or global curvature affect vibrations of such ''flat'' films.

When a smectic film is disturbed by a transverse vibration from its rest shape $z(x,y)$, the resulting deviation $\zeta(x,y,t)$ from the equilibrium state will generate restoring forces implied in the film's equations of motion. The nature and the magnitude of these forces depend on the shape $z(x,y)$ of the film as well as on the structure of the film, that is to say, on the whole set of structures of the N molecular layers in the stack.

In order to be more explicit, let us consider the example of a family of minimal surfaces generated by the contour Γ made of eight mutually orthogonal straight edges, as shown in Fig. 4. Let the length of the horizontal edges be the same, $L_x=L_y=L$. The shape of the surface depends then on the length $L_z=\alpha L$ of the four vertical edges. The minimal sur-

faces spanned on such a frame are known as the so-called T surfaces [14]. Their shape can be calculated numerically using the method of Weierstrass in which the Cartesian coordinates (x,y,z) of the surface are calculated as following integrals:

$$x=\mathrm{Re}\int_{z_0}^{z_l}(1-z^2)R(z)dz,$$

$$y=\mathrm{Re}\int_{z_0}^{z_l}i(1+z^2)R(z)dz,$$

$$z=\mathrm{Re}\int_{z_0}^{z_l}2zR(z)dz, \tag{3.7}$$

where $z=u+iv$ and $R(z)$ is the analytic function of the form

$$R(z)=(z^8-\Psi z^4+1)^{-1/2}. \tag{3.8}$$

When $z_0=0$ (the origin of the complex plane) and z_1 are points from the interior of the circle of radius 1, this algorithm generates T surfaces with the aspect ratio α depending on the value of the parameter Ψ. In the limit $\Psi\Rightarrow\infty$, α tends to 0, and the surface is flat. When Ψ is finite but very large, $\alpha\ll 1$, and one obtains a saddlelike surface which approximate analytic expression is

$$z=\frac{2\alpha(x^2-y^2)}{L}. \tag{3.9}$$

For $\Psi=2$, α tends to infinity, and one obtains the so-called Scherk's $k=1$ surface [13,14]. Such a surface can be seen as composed of two pairs of almost flat and vertical walls connected by a saddle. In the absence of gravitation, the equilibrium position of the saddle is $z(0,0)=0$.

In the fundamental mode of vibrations of such surfaces, the central saddle point moves up and down. In the limit $\alpha=0$ of the flat square film, the eigenmodes and their frequencies are known:

$$\zeta_{mn}(x,y,t)=\zeta_{\max}\cos(\omega_{mn}t)\sin\left(m\,\frac{\pi(x-L/2)}{L}\right)\times\sin\left(n\,\frac{\pi(y-L/2)}{L}\right) \tag{3.10}$$

$$\omega_{mn}=\left(\frac{\tau}{\rho_N}\right)^{1/2}\frac{\pi}{L}\sqrt{m^2+n^2}$$

so that (3.11)

$$\omega_{11}=\left(\frac{2\tau}{\rho_N}\right)^{1/2}\frac{\pi}{L}$$

In the opposite limit $\alpha\gg 1$, the vibration of the surface consists in the motion of the saddle whose approximate mass is $m\approx\rho_N L^2$. The restoring force due to the film tension τ and acting on the saddle can be written as

$$F_z^{\mathrm{ten}}\approx -\tau F\left(\frac{1}{\alpha}\right)\zeta_{00} \tag{3.12}$$

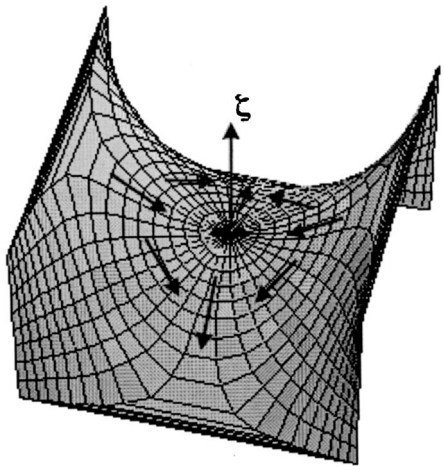

FIG. 5. The displacement ζ of the saddle generates a shear deformation indicated by the arrows.

where $F(1/\alpha)$ is an unknown function. The system looks like a harmonic oscillator of frequency:

$$\omega=\left(\frac{\tau}{\rho_N}\right)^{1/2}\frac{\pi}{L}F\left(\frac{1}{\alpha}\right). \tag{3.13}$$

From Eq. (3.11), we already know that $F(1/\alpha)=2^{1/2}$ in the limit of $\alpha=0$. In the limit of $\alpha\Rightarrow\infty$, the energy of the system cannot depend on the position ζ_{00} of the saddle (when the four vertical edges are *strictly* parallel and equidistant). Therefore, the function $F(1/\alpha)$ must tend to zero. It is crucial to emphasize here that the expression of the restoring force is based on the implicit assumption that the film is liquid and inviscid. Nevertheless, during the ''up and down'' motion of the saddle, the molecules must be transferred between the two pairs of vertical walls that change their lengths. As the amount of the transferred matter is *linear* in ζ, it can generate forces linear in ζ which must be taken into account at the same level of calculations as the restoring force due to the film tension.

When the layers in the film are liquidlike, this transfer is possible by way of a pure shear flow in the saddle region (Fig. 5). In a viscous fluid, such a flow generates viscous stresses which in the limit $1/\alpha\Rightarrow 0$ are of the order of

$$\sigma_{ij}=\frac{\eta h}{2}\left(\frac{\partial v_i}{\partial x_j}+\frac{\partial v_j}{\partial x_i}\right)\approx\eta h\,\frac{\zeta_{00}}{L}\begin{pmatrix}1 & 0\\ 0 & -1\end{pmatrix}, \tag{3.14}$$

where η is the viscosity and v is the flow velocity. These stresses create a difference

$$\Delta\tau\approx\frac{\eta h}{L}\frac{d\zeta_{00}}{dt}=i\omega\,\frac{\eta h}{L}\,\zeta_{00} \tag{3.15}$$

in the film tension between the two pairs of vertical walls and contribute to the restoring force acting on the saddle:

$$F_z^{\mathrm{visc}}\approx i\omega\eta h\zeta_{00}. \tag{3.16}$$

Let us note that as this viscous friction force does not depend on α, the oscillator becomes overdamped and its relaxation time of the order of

$$T_r \approx \frac{\eta h}{\tau F(1/\alpha)} \tag{3.17}$$

diverges in the limit $1/\alpha \Rightarrow 0$.

When the film is crystalline, the vertical displacement of the saddle creates elastic stresses due to the shear deformation

$$\sigma_{ij} = \frac{\mu h}{2}\left(\frac{\partial u_i}{\partial x_j} + \frac{\partial u_j}{\partial x_i}\right) \approx \mu h \frac{\zeta_{00}}{L}\begin{pmatrix} 1 & 0 \\ 0 & -1 \end{pmatrix}, \tag{3.18}$$

where μ is the shear modulus and u is the displacement. The corresponding restoring force is

$$F_z^{\mathrm{el}} \approx \mu h \zeta_{00}. \tag{3.19}$$

Neglecting the contribution of the film tension in the limit $\alpha \Rightarrow 0$, one obtains the frequency of the oscillator:

$$\omega = \left(\frac{\mu h}{\rho_{\mathrm{cl}}}\right)^{1/2} \frac{\pi}{L}, \tag{3.20}$$

independent of the film tension.

Let us now consider in more detail the case $\alpha \ll 1$ of an almost flat surface. During the surface vibration $\zeta(x,y,t)$, each surface element is submitted to inertial and restoring forces that can be elastic and/or dissipative. These forces can be decomposed into the components parallel and perpendicular to the film surface.

In the limit of $\alpha = 0$, the most important are the components orthogonal to the film surface. Indeed, for symmetry reasons, the forces orthogonal to the film must be first order in ζ, while those which are tangent to the film must be second order in ζ. If one considers the trajectories of molecules in the film, and supposes in the first approximation that they are orthogonal to the film surface at each time, then the instantaneous velocity is

$$\vec{v}(\xi_1,\xi_2,t) \approx \frac{\partial \zeta}{\partial t}\vec{n}, \tag{3.21}$$

where $\vec{n}$ is the unit vector normal to the surface and (ξ_1,ξ_2,ξ_3) are the orthonormal coordinates such that ξ_1 and ξ_2 are curvilinear coordinates along the curvature lines of the surface (Fig. 6). The acceleration of this surface element has then two components. The first,

$$a_3 = \frac{\partial^2 \zeta}{\partial t^2}, \tag{3.22}$$

is of the order of $\omega^2 \zeta$, while the second,

$$\vec{a}_{\parallel} = \frac{\partial \zeta}{\partial t}\frac{\partial \vec{n}}{\partial t} = \left(\frac{\partial \zeta}{\partial t}\right)^2 \frac{\partial \vec{n}}{\partial \xi_3}, \tag{3.23}$$

is one order higher in ζ. It has been shown recently that this nonlinear inertial force is at the origin of a large variety of phenomena occurring when the amplitude of vibration is large enough [15]. Here we are interested in the limit of small vibrations, so that the amplitude of motions tangent to the film surface is a second order small quantity.

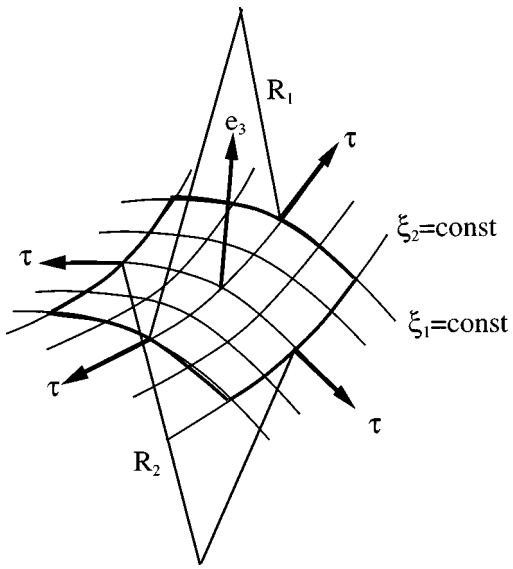

FIG. 6. Definition of curvilinear coordinates ξ_1 and ξ_2. The principal curvature $1/R_1$ is positive, while $1/R_2$ is negative.

When $\alpha \neq 0$, the symmetry with respect to the mirror plane (x,y) is broken so that forces tangent to the film surface may have components which are first order in ζ. However, as these tangent components must be linear in α, they can be made as small as necessary by a proper choice of the out-of-plane deformation.

For these reasons, let us start the search for eigenmodes by considerations of normal forces. We know that the film tension is a source of such a force. As defined in Sec. II, the thermodynamic tension τ provides an isotropic contribution to the stress tensor components tangent to the surface of the film. In the curvilinear orthogonal coordinates (ξ_1,ξ_2,ξ_3), one has

$$N_{ij} = \tau \delta_{ij} \quad \text{for } i,j = 1,2. \tag{3.24}$$

Even if the modulus τ of the tension tensor is uniform throughout the film, it can make a contribution

$$F_3^{\mathrm{cap}} = \tau\left(\frac{1}{R_1} + \frac{1}{R_2}\right) \tag{3.25}$$

to the restoring force in the normal direction when the film has an average curvature during its vibration. At rest, one has $F_3 = 0$, so that the principal curvatures $1/R_{1o}$ and $1/R_{2o}$ must cancel each other:

$$1/R_{1o} = -1/R_{2o} = 1/R_o. \tag{3.26}$$

Due to the displacement $w = w(\xi_1,\xi_2,t)$ in the direction ξ_3 orthogonal to the surface, the changes of the principal curvatures are [12]

$$\frac{1}{R_1} - \frac{1}{R_o} = \frac{1}{A_1}\frac{\partial}{\partial \xi_1}\left(\frac{1}{A_1}\frac{\partial w}{\partial \xi_1}\right) + \frac{1}{A_1 A_2}\frac{\partial A_1}{\partial \xi_2}\left(\frac{1}{A_2}\frac{\partial w}{\partial \xi_2}\right) + \frac{w}{R_o^2}, \tag{3.27}$$

$$\frac{1}{R_2} + \frac{1}{R_o} = \frac{1}{A_2}\frac{\partial}{\partial \xi_2}\left(\frac{1}{A_2}\frac{\partial w}{\partial \xi_2}\right) + \frac{1}{A_1 A_2}\frac{\partial A_2}{\partial \xi_1}\left(\frac{1}{A_1}\frac{\partial w}{\partial \xi_1}\right) + \frac{w}{R_o^2}$$

so that one obtains the restoring force

$$F_3^{\rm cap}=\tau\left(\frac{1}{R_1}+\frac{1}{R_2}\right)=\tau\left(\frac{2w}{R_o^2}+\tilde{\Delta}w\right), \tag{3.28}$$

where

$$\begin{aligned}\tilde{\Delta}=&\frac{1}{A_1}\frac{\partial}{\partial\xi_1}\left(\frac{1}{A_1}\frac{\partial}{\partial\xi_1}\right)+\frac{1}{A_2}\frac{\partial}{\partial\xi_2}\left(\frac{1}{A_2}\frac{\partial}{\partial\xi_2}\right)\\&+\frac{1}{A_1A_2}\frac{\partial A_1}{\partial\xi_2}\left(\frac{1}{A_2}\frac{\partial}{\partial\xi_2}\right)+\frac{1}{A_1A_2}\frac{\partial A_2}{\partial\xi_1}\left(\frac{1}{A_1}\frac{\partial}{\partial\xi_1}\right)\\=&\left(\frac{1}{A_1^2}\frac{\partial^2}{\partial\xi_1^2}+\frac{1}{A_2^2}\frac{\partial^2}{\partial\xi_2^2}\right)-\left(\frac{1}{A_1^3}\frac{\partial A_1}{\partial\xi_1}\frac{\partial}{\partial\xi_1}+\frac{1}{A_2^3}\frac{\partial A_2}{\partial\xi_2}\frac{\partial}{\partial\xi_2}\right)\\&+\frac{1}{A_1A_2}\frac{\partial A_1}{\partial\xi_2}\left(\frac{1}{A_2}\frac{\partial}{\partial\xi_2}\right)+\frac{1}{A_1A_2}\frac{\partial A_2}{\partial\xi_1}\left(\frac{1}{A_1}\frac{\partial}{\partial\xi_1}\right)\end{aligned} \tag{3.29}$$

is the Laplacian operator in curvilinear coordinates (ξ_1,ξ_2). In the above equations, A_1 and A_2 are coefficients of the first fundamental form of the surface:

$$ds^2=A_1^2d\xi_1^2+A_2^2d\xi_2^2. \tag{3.30}$$

The restoring force in Eq. (3.28) has two terms. The first one corresponds to the mean curvature induced by the displacement w of the minimal surface. It would exist even when the displacement w was position independent. Moreover, this term is proportional to the local Gaussian curvature, $1/R_o^2$, of the surface at rest and, consequently vanishes when the surface is flat. The second term contributes to the restoring force when the displacement is position dependent. On a flat surface, where $A_i=1$, the differential operator $\tilde{\Delta}$ becomes the usual Laplacian so that the restoring force equals $-\tau\Delta w$, as expected. On a curved surface, the functions A_i depend on curvilinear coordinates and one has to calculate the corresponding derivatives. Let us take as an example the surface given by Eq. (3.9). For small α, the curvature lines are almost parallel to the x and y axes, so that x and y coordinates play the role of the curvilinear coordinates ξ_1 and ξ_2. In such coordinates, the coefficients of the first fundamental form are

$$A_1^2=1+a^2x^2 \quad \text{and} \quad A_2^2=1+a^2y^2 \tag{3.31}$$

where

$$a=4\alpha/L. \tag{3.32}$$

From Eqs. (3.25), one obtains the restoring force due to the deformation $w=w(x,y)$:

$$\begin{aligned}\frac{F_3^{\rm cap}}{\tau}=&\left(\frac{1}{1+a^2x^2}\frac{\partial^2w}{\partial x^2}+\frac{1}{1+a^2y^2}\frac{\partial^2w}{\partial y^2}\right)\\&-\left(\frac{a^2x}{(1+a^2x^2)^2}\frac{\partial w}{\partial x}+\frac{a^2y}{(1+a^2y^2)^2}\frac{\partial w}{\partial y}\right)\\&+\frac{2a^2w}{[1+a^2(x^2+y^2)]^2}.\end{aligned} \tag{3.33}$$

This has three contributions. In the limit of $a\Rightarrow 0$ (flat film), the two last contributions tend to zero, while the first one tends to the usual Laplace term $\tau\Delta w$, as expected. On a square frame of the size L^2, its order of magnitude depends on the wave vector of the eigenmode. For $w=w_o(t)\sin(m\pi x/L)\sin(n\pi y/L)$, one gets $\Delta w=-(m^2+n^2)\times(\pi/L)^2w$. When the film becomes curved, one has to compare this term with the two other ones which, respectively, are of the order of $a^2L(m^2+n^2)^{1/2}(\pi/L)w$ and a^2w. The factor a^2 in these two terms corresponds to the Gaussian curvature of the surface:

$$\frac{1}{R_o^2}\approx a^2=\alpha^2\frac{16}{L^2}. \tag{3.34}$$

Therefore, as long as the principal curvature of the film $1/R_o\approx a$ is much smaller than the wave vector $(m^2+n^2)^{1/2}(\pi/L)$ of the eigenmode, the Laplacian term dominates and the correction due to the Gaussian curvature is second order in α. Besides the restoring forces due to the isotropic static tension of the film, one has to examine forces due to stresses induced by in-plane strains of the vibrating film. Indeed, it is well known from the theory of thin shells that the deformation $w(\xi_1,\xi_2)$ orthogonal to the film surface induces the in-plane strains [12]:

$$\varepsilon_{11}=\frac{w}{R_1}, \quad \varepsilon_{22}=\frac{w}{R_2} \quad \text{and} \quad \varepsilon_{12}=\varepsilon_{21}=0. \tag{3.35}$$

On a minimal surface, these deformations are traceless because $1/R_1=-1/R_2=1/R_o$. Therefore, as expected, there is no change in the surface area of the film and the deformation is a pure shear. When the film is liquid, as in SmA or SmC phases, the shear rate generates viscous stresses:

$$\sigma_{ij}^{\rm visc}=\eta h\dot{\varepsilon}_{ij}=\eta h\frac{\dot{w}}{R_o}\begin{pmatrix}1&0\\0&-1\end{pmatrix} \tag{3.36}$$

while, when the film is crystalline, like in the Sm$B_{\rm cryst}$ phase, the shear deformation generates elastic stresses:

$$\sigma_{ij}^{\rm el}=\mu h\varepsilon_{ij}=\mu h\frac{w}{R_o}\begin{pmatrix}1&0\\0&-1\end{pmatrix}. \tag{3.37}$$

These in-plane stresses generate the normal force

$$F_3^{\rm el}=\left(\frac{\sigma_{11}}{R_1}+\frac{\sigma_{22}}{R_2}\right)\approx 2\mu h\frac{w}{R_o^2} \tag{3.38}$$

in an elastic film, and

$$F_3^{\rm visc}=\left(\frac{\sigma_{11}}{R_1}+\frac{\sigma_{22}}{R_2}\right)\approx 2i\omega\eta h\frac{w}{R_o^2} \tag{3.39}$$

in a viscous film.

Let us note that expressions (3.38) and (3.39) are similar to the first term in expression (3.28) of the force due to the thermodynamic tension τ of the film. In all three cases one finds the same term w/R_o^2 multiplied by different prefactors: τ for the isotropic tension, $\tau_\mu=2\mu h$ for the elastic response, and $i\tau_\eta=2i\omega\eta h$ for the viscous one. The typical tension of smectic films is of the order of 50 dyn/cm. For the shear

elastic modulus of crystalline film of the order of 10^8 dyn/cm^2, one obtains $\tau_\mu \approx 10^2$ dyn/cm for a two-layer film, 10^3 dyn/cm for a 20-layer film, and 10^4 dyn/cm for a 0.5-μm-thick film. For $\omega \approx 2000\ s^{-1}$ and $\eta \approx 1$ P, the viscous contribution τ_η is only of the order of 2×10^{-3} dyn/cm for a two-layer film. In conclusion, the shear deformation in curved films is expected to have significant effects on eigenmodes in crystalline thick films, but can be neglected in liquid films.

In order to estimate the effects of the Gaussian curvature on the eigenmodes, let us introduce the forces given by Eq. (3.38) in the equation of motion of a film submitted to a deformation $w(x,y,t)$ in the direction ξ_3:

$$\rho \frac{\partial^2 w}{\partial t^2} = \tau \Delta w + \frac{w}{R_o^2}(2\tau + 2\mu h). \tag{3.40}$$

In the approximation where R_o is considered as small and *position independent*, the eigenmodes of this differential equation are the same as the ones for the flat film [Eqs. (3.8) and (3.9)], and one obtains the dispersion equation

$$\rho \omega_{mn}^2 = \tau q_{mn}^2 + \frac{2\tau + 2\mu h}{R_o^2}, \tag{3.41}$$

where

$$q_{mn}^2 = \pi^2 \left(\frac{m^2}{L_x^2} + \frac{n^2}{L_y^2} \right). \tag{3.42}$$

In agreement with the heuristic arguments from the beginning of this section, one finds that the global Gaussian curvature of the film increases the frequency of the eigenmodes in the case when the film possesses an in-plane shear elasticity. The shift of the frequency squared is proportional to the product of the global Gaussian curvature and of the elastic shear modulus of the film.

IV. EXPERIMENTAL SETUP

The general view of the experimental setup is presented in Fig. 7. This setup is roughly similar to the one used in previous studies [16], but the frame on which the smectic films are spanned is new, to our knowledge. It is presented in detail in Fig. 8.

The smectic film is held on a rectangular metallic frame with two sides fixed and two sides mobile. As shown in Fig. 8, the two fixed sides have V-shaped, 90°, sharp linear edges E_1 and E_2 playing two roles. First, they serve as rails for the two mobile parts of the frame fitted on these edges by means of 90° notches. Moreover, they constitute two linear segments of the film boundary, which is completed by the edges E_3 and E_4 of the mobile parts.

In the case when these mobile edges are V-shaped, linear, and, by construction, put in the same plane as the fixed edges, the whole boundary is, in principle, a plane rectangle and the held film should be flat [Fig. 8]. In practice, one always observes deviations from such an ideal flat shape mainly for two reasons:

1°—First of all, as we saw in Sec. III, the film is connected to the frame via the meniscus containing much more

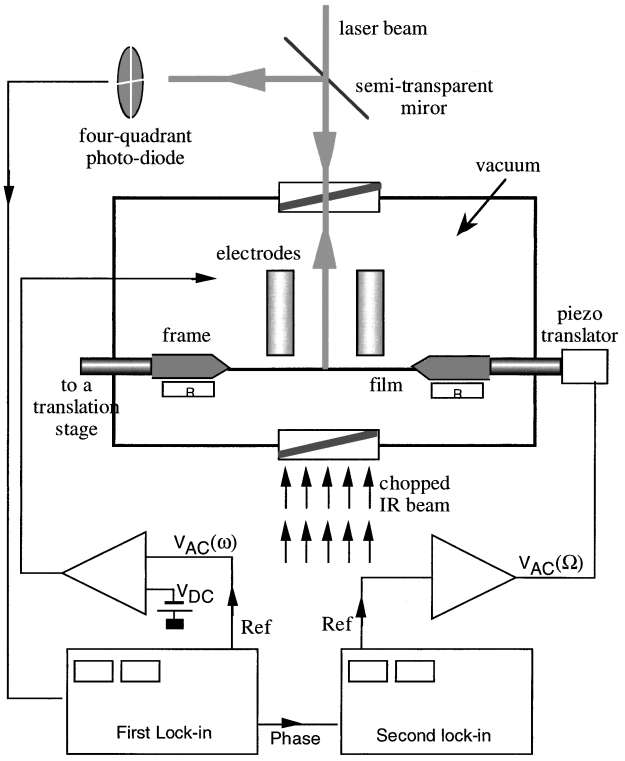

FIG. 7. Experimental setup.

of the liquid crystal (LC) substance than the film itself. Without annealing the sample slightly below the SmA–nematic transition temperature, the distribution of the LC in the meniscus and, consequently, its shape vary on the scale of few tenths of a mm, so that the film presents corrugations localized along its boundary. These corrugations are well visible in the reflecting microscope, as they show a quite strong intensity variations.

2°—After annealing the sample, these localized corrugations disappear but the film keeps always a global Gaussian curvature due to unavoidable mechanical imperfections of the frame. This global curvature shows as (and can be deduced from) an elliptical modification of the shape of the laser beam reflected on the film.

Once we started to suspect that these accidental curvatures modify vibrations of the smectic film in crystalline phases, even if they are small, we decided to amplify and control them by means of two different modifications of the frame.

In order to introduce the localized curvature, the edges E_3 and E_4 of the frame have been made sinusoidal shaped using corrugated stripes of a thin copper sheet soldered to the linear edges of the standard V-shaped mobile parts of the frame [see Fig. 8(c)]. Let us note that the corrugations present on opposite edges fit precisely one to the other, so that such a modified frame can be closed completely and the procedure of drawing a film is identical to the one using the standard frame [7,8].

The global Gaussian curvature of the film has been obtained simply by a change in the height of the mobile linear edges E_3 and E_4 with respect to the fixed edges E_1 and E_2 [see Fig. 8(b)]. Let as note that the frame modified in such a manner cannot be completely closed; when the edges E_3 and

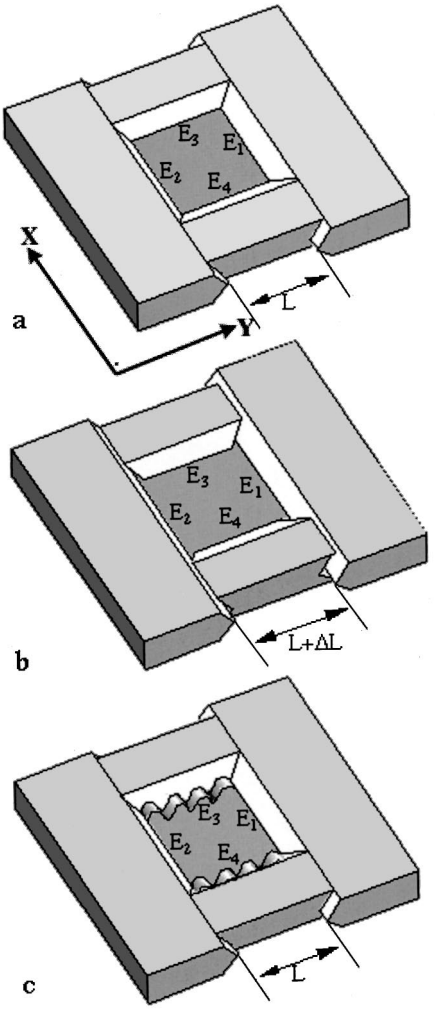

FIG. 8. Frames: (a) Planar rectangular frame. (b) Out-of-plane frame; the edges E_3 and E_4 are lower than E_1 and E_2 due to the lateral shift ΔL. (c) Frame with crumpled edges E_3 and E_4.

E_4 are in contact, open spaces persist at their extremities. In order to pull a film, these holes must be carefully filled with an extra amount of the LC material.

The frame is installed in a metallic cell fixed to the translation stage of the reflecting microscope. The cell of a quite complex structure plays several roles.

1°—It has a removable cover fixed to the base part by means of six screws. When the cell is open, all manipulations necessary for deposition and distribution of the LC material on the frame are possible.

2°—When closed, the cell is tight, thanks to the *o* ring situated between the cover and the base, and it can be submitted to vacuum.

3°—The cell is equipped with two axles screwed to the mobile parts of the frame. Both axles glide in tight *o* rings equipped with bearings, and can be manipulated from the exterior of the cell by means of translation stages. Therefore, smectic films can be drawn and their dimensions can be changed with the cell closed.

4°—One of the axles is connected to a piezo translator, so that dimensions of the frame can be modulated with accuracy in the micrometer range.

5°—The cell is equipped with oblique glass windows for direct observations and for detection of the film motion by means of a laser beam. The bottom window allows also a passage of a chopped IR beam used for the purpose of a periodic modulation of the film's temperature.

6°—The mean temperature of the cell is regulated using two electric heaters situated in the base and in the cover of the cell. Moreover, the fixed parts of the frame are equipped with two other heating elements, so that the temperature of the frame is controlled independently and can be made higher than the one of the cell. As we will see below, this is very useful when one wants to avoid film damages caused by phase transitions. The temperature regulation thus obtained is better than $\pm 0.03\,^{\circ}\mathrm{C}$.

7°—The cover of the cell holds a system of four electrodes that have been machined from a single copper block in order to control as well as possible their geometry. These electrodes can be translated vertically by means of two coupled rods gliding in *o*-ring-equipped bearings situated within the cover. In their ''up'' position, the electrodes are far enough from the frame to allow the motion of the mobile edges during pulling of the film. Once the film has been drawn, the electrodes are lowered and approached to the film as close as about 0.1 mm.

The four electrodes can be supplied independently with voltages $V_i = V_{\mathrm{dc}} + V_{i\mathrm{ac}}$ $(i = 1, \ldots, 4)$ having dc and ac components.

The dc component V_{dc} of about 50 V is identical for all electrodes. Its role is to charge the capacitor consisting of these four electrodes, and of the film whose conductance is very low but which behaves effectively as a conductor at time scale longer than 30 s. The surface density of charges σ_{dc} brought by this dc field on the film is proportional to the capacity C and to the dc voltage,

$$\sigma_{\mathrm{dc}} \sim C V_{\mathrm{dc}}. \tag{4.1}$$

These dc charges are submitted to the alternating field created by the ac components of the voltage applied to the electrodes. It can be either $V_{\mathrm{ac}} \sin(\omega t)$ (coming directly from the internal generator of the lock-in amplifier) or $-V_{\mathrm{ac}} \sin(\omega t)$ (produced by a voltage invertor). The geometry of the electric field created by the ac voltage is mainly defined by the distribution of grounded metallic parts in the cell, because the presence of a very resistive film can be ignored due to the high enough frequency ω. The ac electric field is the most intense in the vicinity of the electrodes, to which it is orthogonal. In conclusion, the dc charges distributed in the film (mainly below the electrodes) are submitted to forces proportional to the ac voltages:

$$f \sim C V_{\mathrm{dc}} E_{\mathrm{ac}} \sim C V_{\mathrm{dc}} V_{i\mathrm{ac}}. \tag{4.2}$$

Using different combinations of the ac voltages, several eigenmodes of the film can be excited selectively. For example, in order to excite the fundamental mode (1,1), all four electrodes are connected to the same source of the ac voltage (also see Sec. V). In order to excite selectively the (1,2) and (2,1) modes, adjacent electrodes are connected in pairs, respectively, *AB-CD* and *AD-BC* (see Fig. 7).

Vibrations of the film are detected optically using the system shown in Fig. 7. The He-Ne laser beam reflected from an appropriate portion of the film (the portion where, for a given

mode, the excursion of the film slope is the largest) is sent on a quadrant photodiode which detects its motions. The differential signal $I(\omega)$ coming from the photodiode and synchronous with the exciting ac voltage is analyzed by the first lock-in.

The first eigenmodes of the film usually being very slightly damped (in air, the damping is mainly due to the viscous dissipation of air currents), the signal $I(\omega)$ shows quite sharp resonances with well defined eigenfrequencies $\omega_{n,m}$. In order to track the evolution of the resonance frequency of one of the eigenmodes as a function of temperature, the phase output ϕ of the first lock-in is used as the error signal. Necessary corrections of the excitation frequency are calculated from this, and are sent to the lock-in signal generator by a computer that also deals with all other tasks such as temperature control and data accumulation.

Let us note that the precision of this resonance tracking method is limited by the accuracy of the frequency definition of the lock-in generator which is 0.1 Hz in the range 100–1000 Hz and 1 Hz in the range 1–10 kHz.

Once the excitation frequency is corrected back to its resonance value ω_{nm}, the slope $\Delta\phi/\Delta\omega$ of the phase ϕ vs the frequency is determined from measurements of the phase for frequencies $\omega_{nm}+10$ Hz and $\omega_{nm}-10$ Hz.

In some experiments, due to the modulation of the frame surface or film temperature, the film tension and, consequently, the frequency of the eigenmodes, oscillate slowly around its equilibrium value. The typical modulation frequency Ω of about 1 Hz is lower than the eigenmode frequency by two orders of magnitude at least. The amplitude $\Delta\omega_{nm}(\Omega)$ and the phase $\Psi_{nm}(\Omega)$ of this vibrato is detected by the second lock-in, and has the phase output ϕ of the first lock-in as an input. Indeed, one has

$$\Delta\omega_{nm}(\Omega)=\frac{\Delta\phi_{nm}(\Omega)}{\left(\frac{d\phi}{d\omega}\right)} \tag{4.3}$$

where $\Delta\phi_{nm}(\Omega)$ and $d\phi/d\omega$ are, respectively, the excursion of the phase and the phase slope detected by the first lock-in.

V. EXPERIMENTAL RESULTS

As stated at the beginning of Sec. III the rigidity with respect to the bending of crystal-like smectic films should be influenced by their Gaussian curvature. In order to prove the validity of this generic idea by a simple but nevertheless crucial experiment, we first used a frame with sinusoidal-shaped mobile edges. In this case, the Gaussian curvature is localized in two bands of approximate width λ, parallel to the deformed edges. The corresponding increase in the bending rigidity of the film should be localized there. In practice, this means that when the film becomes crystalline, these two peripheral bands where the film is strongly curved should be excluded from vibrations. As a consequence, the film should behave as if it was shorter in the direction orthogonal to the crimped edges, and the frequency ω_{mn} of its eigenmodes should rise.

Results of this crucial experiment are shown in Figs. 9 and 10. In Fig. 9 are plotted four resonance peaks corresponding to the first four eigenmodes of a $7O.7$ film drawn

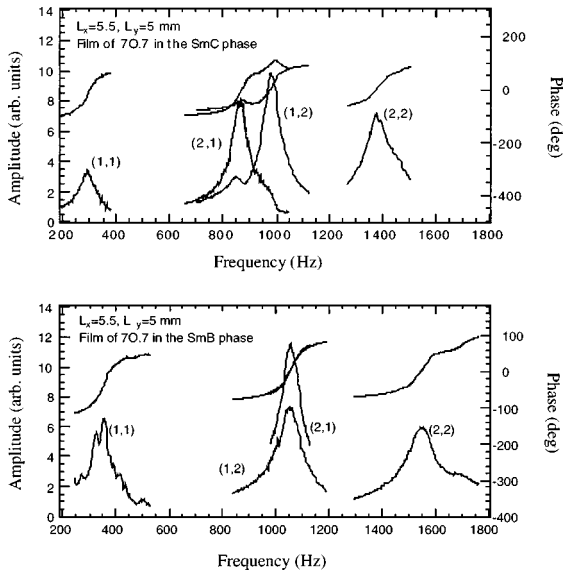

FIG. 9. Spectra of the first four eigenmodes in the SmC and SmB phases. The frequency shift at the Sm$C\Rightarrow$SmB transition of the (2,1) mode is larger than the one of the (1,2) mode. This difference is due to the curvature localized in the vicinity of the corrugated L_y edges.

on a rectangular frame ($L_x=5.5$ mm and $L_y=5.0$ mm). In the SmC-like phase [Fig. 9(a)], the resonance frequency of the (2,1) mode is lower than that of the (1,2) mode. This is due to the fact that the smectic layers are liquidlike, so that the localized Gaussian curvature has almost no effect on the film vibrations, as discussed in Sec. III. At lower temperature, when the film is in the SmB-like phase [Fig. 9(b)], the frequencies of all four eigenmodes are higher than the corresponding ones recorded in the SmC-like phase, but the frequency shift is much larger for the (2,1) mode than for the (1,2) mode. These results are summarized in Fig. 10 where the frequencies f_{mnC} of the four eigenmodes in the SmC-like phase are plotted versus corresponding frequencies f_{mnB} of the eigenmodes recorded in the SmB-like phase (crosses).

This anisotropic behavior of the (1,2) and (2,1) eigenmodes at the Sm$C\Rightarrow$SmB_{cryst} phase transition constitutes a suitable proof of the rigidifying action of the curvature. In-

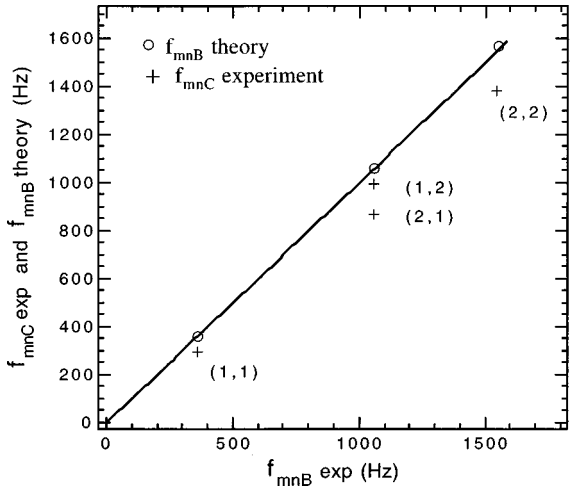

FIG. 10. Fit of the experimental results using Eq. (5.4).

deed, the distribution of the Gaussian curvature in the film is anisotropic. The curvature is localized in two bands orthogonal to the x axis, so that the effective L_x dimension of the film is shortened under the Sm$C \Rightarrow$ SmB transition while the L_y dimension remains unchanged. Quantitatively, the frequency of the (m,n) eigenmodes in the SmC-like phase is expected to obey the Rayleigh-type expression:

$$f_{mnC}^2 = \frac{\tau_C}{4\rho_{mnC}} \left[\left(\frac{m}{L_{xC}} \right)^2 + \left(\frac{n}{L_{yC}} \right)^2 \right], \tag{5.1}$$

where $L_{xC} = L_x$ and $L_{yC} = L_y$. The density ρ_{mnC} is an effective quantity taking into account not only the mass of the smectic film but also the mass of the air surrounding the film, and that is put into motion by the vibrating film. As the mass of the air participating in the film vibrations depends on the shape of the eigenmode, the effective density ρ_{mnC} depends on the indices (m,n). Introducing the air density ρ_{air} and the effective thickness of the air layer H_{mn}, the effective 2D density can be written as

$$\rho_{mnC} = \rho_{\text{air}} H_{mn} + \rho_{\text{cl}} h, \tag{5.2}$$

where h is the film thickness.

In the SmB phase, expression (5.1) is modified according to Eq. (3.40) by the addition of the curvature dependent term

$$f_{mnB}^2 = \frac{\tau_B}{4\rho_{mnB}} \left[\left(\frac{m}{L_{xB}} \right)^2 + \left(\frac{n}{L_{yB}} \right)^2 \right] + f_p^2, \tag{5.3a}$$

where

$$f_p^2 = \frac{1}{(2\pi)^2} \frac{2\mu h}{\rho_{mnB} R_o^2}. \tag{5.3b}$$

In agreement with our model, the L_y dimension of the film stays unchanged, $L_{yB} = L_y$, while $L_{xB} = L_x - \Delta L$ is shortened by the ripples. From the above two equations one obtains the following relation:

$$f_{mnB}^2 = f_{mnC}^2 \frac{\tau_B}{\tau_C} \left[\left(\frac{m}{L_x - \Delta L} \right)^2 + \left(\frac{n}{L_y} \right)^2 \right] \Big/ \left[\left(\frac{m}{L_x} \right)^2 + \left(\frac{n}{L_y} \right)^2 \right] + f_p^2 \tag{5.4}$$

between the frequencies of eigenmodes in SmC- and SmB-like phases. This contains three adjustable parameters. The first one is the ratio τ_B/τ_C between the film tensions in the SmB-like and SmC-like phases respectively. It is expected to be of the order of 1. The second parameter is the ripple-induced reduction ΔL of the film length in the SmB-like phase. It should be of the order of the ripple wavelength, i.e., $\lambda = 0.1$ cm. Finally, there is the frequency shift f_p due to the global Gaussian curvature of the film. As noted in Sec. II, one cannot exclude its existence due to small accidental imperfection of the frame geometry. With the choice of the three adjustable parameters $f_p = 134$ Hz, $\Delta L = 0.1065$ cm, and $\tau_B/\tau_c = 1.03$, the theoretical values of the frequencies f_{mnB} are calculated from Eq. (5.4) and plotted in Fig. 11 versus the measured frequencies f_{mnB}. The data computed (open circles) are aligned on a straight line of slope 1.

Besides the confirmation of the expected rigidifying role of the localized ripples, this experiment and several other similar experiments show that, even when the accidental global film curvature is small, it plays an important role in film vibrations in the SmB-like phase.

In order to understand better the role of the global curvature in different mesophases, a long series of experiments was performed on 7O.7 films of various thicknesses drawn on the out-of-plane frame with straight edges [Fig. 8(b)]. The effective radius of curvature in the center of those films was estimated from the shape of the reflected laser beam to be $R_o \approx 20$ cm.

All films were drawn first in the SmA-like phase. In order to determine their thickness h, the frequency f_{12A} of their (1,2) mode was measured in vacuum. The typical plot of the vibration amplitude and phase versus the excitation frequency is shown in Fig. 11. Knowing the value of the resonance frequency f_{12}, the dimensions of the frame ($L_x = 0.5$ cm and $L_y = 0.59$ cm), the liquid crystal density $\rho \approx 1$ g/cm^3, and the film tension $\tau \approx 50$ dyn/cm, the film thickness h was determined from Eq. (5.2) with the 2D mass density set to $\rho_{mn} = \rho h$.

After the thickness determination, the air was introduced into the sample cell again, and all other measurements were made in the air atmosphere. Except for very thick films, the effective density $\rho_{mn} = \rho_{\text{cl}} h + \rho_{\text{air}}$ is dominated by the contribution of the air participating in the vibrations of the film, so that effects due to changes in the film density as a function of the temperature can be neglected.

For each film, four different quantities were measured as a function of temperature during a slow cooling from $T_u \approx 68$ °C to $T_1 \approx 35$ °C. The typical scan rate was $dT/dt \approx -0.1$ °C/60 s. The two plots shown in Fig. 12 concern two parameters of the (1,2) eigenmode: its resonance frequency $f_{12}(T)$ and the phase slope $\Delta\phi/20$ Hz measured as explained in Sec. IV. The two other plots in Fig. 13 concern the response of the eigenmode frequency to thermomechanical stresses induced in the film by an IR beam modulated at a low frequency of 1.2 Hz. It is important to note that during these temperature scans, the frame was slightly heated (see Sec. IV) in order to introduce a small radial temperature gradient in the film. The purpose of this temperature gradient was crucial: Due to the radial temperature gradient, the SmB-like phase always nucleates in the center of the SmC-like film during the phase transition, and grows by a slow outward propagation of the phase boundary. During such directed growth of the SmB-like phase, the density dis-

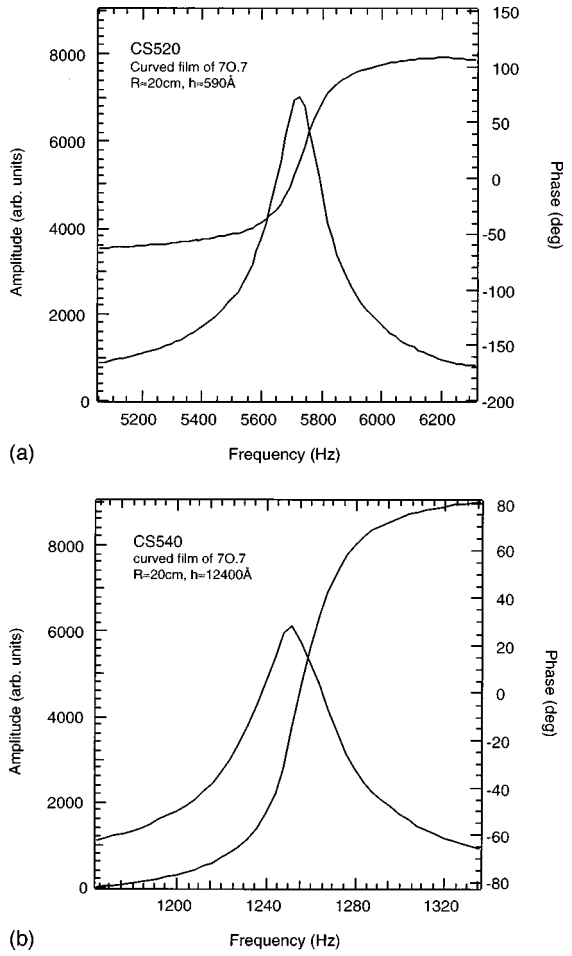

FIG. 11. Spectra of the (1,2) mode recorded in vacuum for films of different thicknesses. Knowing the dimensions of the film and the density of the liquid crystal, the thicknesses $h=590$ and 12 400 Å of films have been determined from the resonance frequencies.

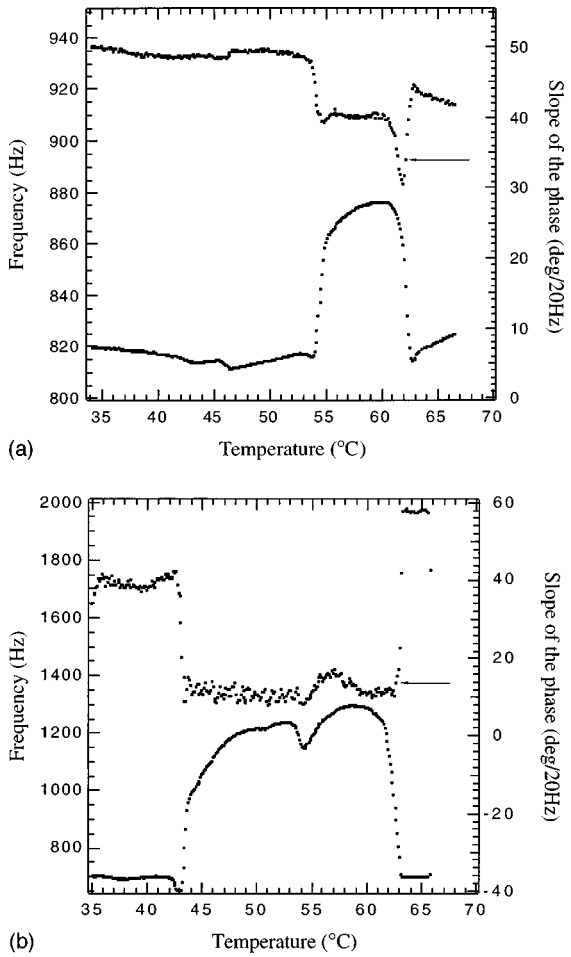

FIG. 12. Frequency of the eigenmode (1,2) and the slope of the phase at the resonance plotted as a function of the temperature. Note differences in the range of temperatures for which, due to the SmB crystalline structure, the frequency of the (1,2) eigenmode is shifted with respect to its level in the SmC phase.

continuity $\Delta\rho$ between the SmB- and SmC-like phases generates a mass flow of molecules from the meniscus to the moving phase boundary. Due to the persistent fluidity of the meniscus which is still in the liquid SmC-like phase, such a mass flow is possible without generation of the destructive mechanical stresses that would have appeared in the opposite case if the meniscus became frozen (SmB) before the main body of the film. All four plots in Figs. 12 and 13 show anomalies coinciding with phase transitions in the film.

The main feature of the plot $f_{12}(T)$ is the increase of about 20% in the resonance frequency f_{12} in the SmB-like phases with respect to all other phases. The height $\Delta f_{12}=f_{12B}-f_{12C}$ of the frequency jump at the Sm$C\Rightarrow$SmB transition depends on the film thickness [compare Figs. 12(a) and 12(b)], as shown in Fig. 14 (filled circles). The two other plots of this figure show the variations of the frequencies f_{12C} and f_{12B} with the film thickness h.

Following Eq. (5.1), the observed variation of $f_{12C}(h)$ in the SmC phase can only be due to the variation of the effective density ρ_{mnC} with the thickness [Eq. (5.2)] because it is known that the film tension varies very little with the film thickness [4]. Using this assumption, the experimental data were fitted to the expression

$$f_{12C}(h)=f_o/\sqrt{1+h/h_o}, \tag{5.5}$$

with two adjustable parameters

$$f_o^2=\frac{\tau_C}{4\rho_{\mathrm{air}}H_{12}}\left[\left(\frac{1}{L_x}\right)^2+\left(\frac{2}{L_y}\right)^2\right] \tag{5.5a}$$

and

$$h_o=\frac{\rho_{\mathrm{air}}}{\rho_{\mathrm{cl}}}H_{12}. \tag{5.5b}$$

The parameter h_o corresponds to the film thickness in the case where the inertia of the film and of the air are the same. The values extracted from the fit are $f_o=830$ Hz and $h_o=2500$ nm. Knowing h_o and the ratio $\rho_{\mathrm{air}}/\rho_{\mathrm{cl}}\approx 10^{-3}$, one obtains the effective thickness of the air layer: $H_{12}=2.5$ mm. This value is in agreement with the crude estimate based on the air flow pattern in the vicinity of the film. From f_o, H_{12}, the air density $\rho_{\mathrm{air}}=10^{-3}$ g/cm^3 and the film dimensions ($L_x=0.5$ cm, $L_y=0.59$ cm), one obtains $\tau_C=45$ dyn/cm, in agreement with typical values of the film tension [6,7,18].

In the SmB-like phase, the experimental data in Fig. 14 show that the (1,2) eigenfrequency increases with thickness, unlike with the SmC-like phase. Following Eq. (5.3), this

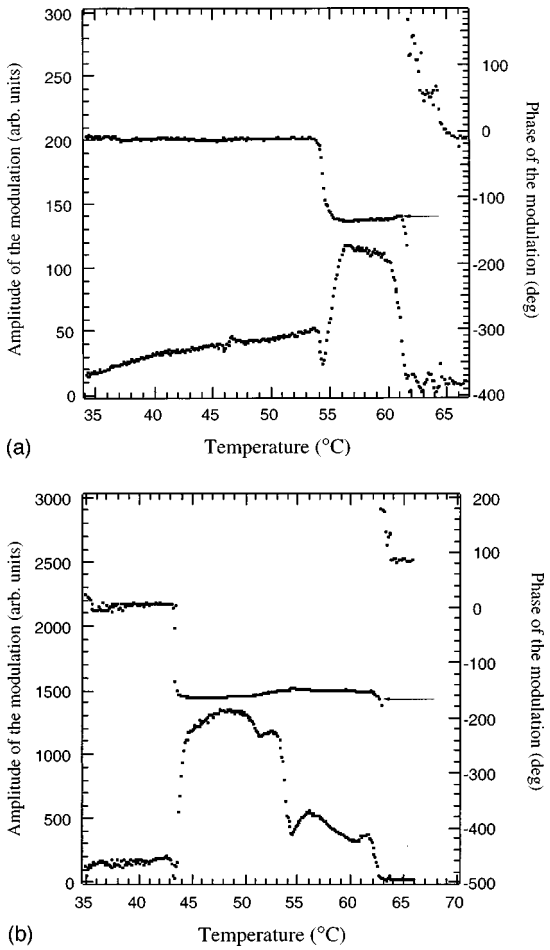

FIG. 13. The film is submitted to a chopped IR light beam. The frequency of the eigenmode (1,2) is modulated due to thermomechanical stresses induced by IR heating. The amplitude and phase of this modulation measured with the second lock-in are plotted as a function of the temperature.

means that the effect of the in-plane shear elasticity modulus μh of the SmB-like phase overcomes the action of the effective density rise. The experimental data were fitted to the expression

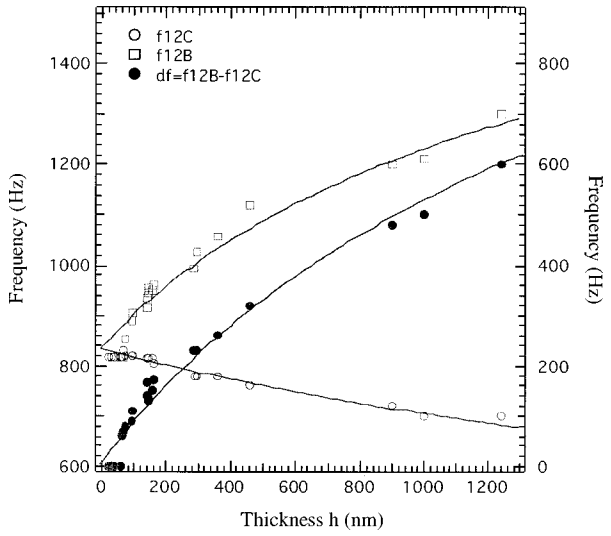

FIG. 14. Frequency jump of the (1,2) mode at SmC⇒SmB transition as a function of the film thickness.

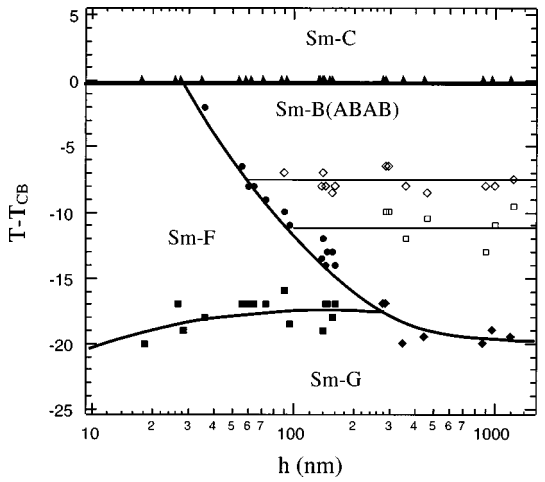

FIG. 15. Phase diagram of temperature vs thickness of 7O.7 films established from singularities occurring in plots shown on Figs. 12 and 13. Note the presence of stacking transitions in the SmB phase. Lines on this diagram are only guides to the eye.

$$f_{12B}(h)=\sqrt{f_o^2+ah}/\sqrt{1+h/h_o}, \tag{5.6}$$

where the meanings of f_o and h_o are the same as above, while the meaning of the parameter a is given by Eq. (5.3):

$$a=\frac{1}{(2\pi)^2}\frac{2\mu}{\rho_{nmB}R_o^2}.$$

Its value determined from the fit is $a=1.5\times10^7\ \mathrm{s}^{-2}\,\mathrm{cm}^{-1}$. Using $\rho_{12B}=2.5\times10^{-3}$ g/cm^2 and $R_o\approx20$ cm, one obtains $\mu\approx10^8$ dyn/cm^2, in agreement with the expected value of the shear modulus in the SmB phase.

VI. DISCUSSION

Besides the positive shift of the (1,2) eigenfrequency when entering the SmB phase, the plots of Figs. 12 and 13 contain several other interesting features.

Range of the SmB phase: Most obviously, the width ΔT_B of the temperature range in which this shift occurs depends on the film thickness. It is about 7.5 °C for a 590-Å-thick film and 20 °C for a 12 400-Å-thick film. For films thinner than 300 Å, a frequency jump does not occur, which can be interpreted as due to the absence of the SmB phase. In the phase diagram of Fig. 15, the upper limit of the SmB phase is plotted using filled triangles, while the lower limit is indicated with filled circles (SmB⇒SmF phase transition—see below) or diamonds (SmB⇒SmG phase transition).

Stacking transitions: As reported in Ref. [11] several stacking transitions occur in the range of the SmB phase in 7O.7. These stacking transitions are visible on plot 13(b) showing the modulation of the eigenmode frequency due to thermomechanical stresses induced by the IR chopped beam. One notes two changes in the amplitude level: one at 52 °C and one at 54 °C. These features are plotted as open diamonds, squares, and triangles on the phase diagram of Fig. 15.

Presence of the SmF phase: For thicknesses between 300 and 2000 Å, the SmB phase is partially (depending on the thickness) replaced by the SmF phase. Due to the absence of

the crystalline order, the shear modulus of this phase is zero, so that the frequency of the (1,2) eigenmode recovers the level of the Sm*C* phase. The lower limit of the temperature range of the Sm*F* phase (filled squares on the phase diagram of Fig. 15) has been determined from small irregularities such as those visible in plots of Figs. 12(a) and 13(a) around 45 °C.

Shear modulus of the SmG phase: The Sm*G* phase is known to possess a crystalline order but, in contradistinction with the Sm*B* phase, the frequency of the (1,2) eigenmode is not shifted [see Fig. 12(b)]. The explanation of this paradox was given in Ref. [16]. In the Sm*G* phase, molecules are tilted with respect to the layers normal. The tilt angle is an additional degree of freedom used by the system in response to changes in the in-plane distances between molecules. For this reason, the in-plane elastic moduli of the Sm*G* phase are smaller by a factor of the order of 10^2 with respect to those of the Sm*B* phase.

In-plane thermal dilation: The tilt angle also plays a crucial role in thermal dilation. As shown in Fig. 13(b), the phase of the thermally induced modulation of the eigenmode frequency has a π change at the Sm$B \Rightarrow$SmG phase transition. This means that, for example, under an increase in temperature, the thermomechanical stresses are compressive in the Sm*B* phase and tensile in the Sm*G* phase. This is due to the fact that molecules are normal to the layers in the Sm*B* phase, so that they can respond only by a change of their intermolecular distances when the temperature changes. As a result, under heating, the 2D density of the Sm*B* phase would decrease if the surface area of the film could change. In the Sm*G* phase, the tilt angle depends on the temperature. It decreases under heating, so that the 2D density of the Sm*G* phase would increase if the surface area of the film could change.

Temperature vs thickness phase diagram: The phase diagram established from all these features is shown in Fig. 15. Let us note that the *Y* axis indicates the reduced temperature $T - T_{CB}$ with respect to the Sm$C \Rightarrow$SmB (or SmC/SmF) phase transition temperature T_{CB}. The reason for such a choice is that our experiments were performed in air on a day times scale (typical length of a run) so that the phase transition temperatures showed some shifts due to the degradation of the liquid crystal. In spite of this lack of knowledge of the absolute temperatures, we can conclude that the diagram of Fig. 15 is very similar to the one established from x-ray studies by Sirota *et al.* [11].

VII. CONCLUSIONS

In the present work, it has been shown both theoretically and experimentally that in-plane crystalline elasticity increases the frequency of eigenmodes of smectic films when they are curved and, more precisely, when they possess a Gaussian curvature. The frequency shift with respect to the pure-capillary case (Sm*A* or Sm*C* phases) was found to be proportional to the product of the effective in-plane shear modulus μh, and of the global Gaussian curvature $1/R_o^2$.

Let us note that the theoretical model used here was oversimplified because, in the search for the eigenmodes of the equation of motion [Eq. (3.40)], the Gaussian curvature was supposed to be position independent. This is a crude approximation because, in general, the Gaussian curvature varies from one point of a minimal surface to another and therefore depends on the two curvilinear coordinates (ξ_1, ξ_2), except for the case of the catenoide. As pointed our recently by Ben Amar and da Silva [17], the Gaussian curvature does not depend on the azimuthal angle, due to the symmetry of revolution.

In light of this remark, one could say that the shapes of smectic films used in our experiments were too complex from a theoretical point of view. However, our aim was to explain some surprising results obtained previously with a rectangular planar (in principle) frame [8]. This is the reason why frames used here were obtained by simple modifications of the rectangular planar one. For future experiments, a ''tilted square'' frame made of four oblique straight segments seems to be the most suitable. Within such a frame, the minimal surface can be approximated as a simple saddle [Eq. (3.9)], and its Gaussian curvature can be controlled by changes in the tilt angle.

As the frequency shift due to the Gaussian curvature is proportional to the in-plane shear elastic modulus of the smectic film, its measurements as a function of temperature allowed us to detect phase transitions. In particular, the stacking transitions, discovered previously by Sirota, Pershan, and Deutsch [11] in the Sm*B* phase, have been detected.

The signature of the stacking transitions has also been found in experiments where the modulation of the (1,2) eigenmode was induced by a low frequency periodic heating of smectic films with an IR beam. These experiments show that the sign of the in-plane thermomechanical stresses is inverted, with respect to the Sm*B* phase, in the Sm*G* and Sm*F* phases. We interpreted this effect as due to the presence of the molecular tilt, which decreases with temperature and leads to an in-plane contraction under heating.

In conclusion, the drumhead vibrations of smectic films have been shown to be very sensitive to their structures when the films have a built-in Gaussian curvature. This allowed us to detect phase transitions and to establish a phase diagram of temperature vs thickness similar to the one of Ref. [11]. Further progress in the quantitative interpretation of the measurements requires exact calculations of the eigenmodes. This seems to be difficult in cases where the Gaussian curvature *K* depends on the two curvilinear coordinates of the surface. The case of a catenoid seems simpler, since *K* depends only on one of the isothermal coordinates.

ACKNOWLEDGMENTS

We thank Cécile Durost and Sandrine Lemonnier for a very useful collaboration.

[1] Mark Kac, Am. Math. Monthly **73**, 1 (1966).
[2] C. Gordon, D. Webb, and S. Wolpert, Bull. Am. Math. Soc. **27**, 134 (1992).
[3] S. Sridhar and A. Kudrolli, Phys. Rev. Lett. **72**, 2175 (1994).
[4] C. Even and P. Pieranski, Phys. Rev. E (to be published).
[5] H. Wu, D. W. Sprung, and J. Martorel, Phys. Rev. E **51**, 703 (1995).
[6] K. Miyano, Phys. Rev. A **26**, 1820 (1982).
[7] P. Pieranski, L. Belliard, J.-Ph. Tournellec, X. Leoncini, C. Furtlehner, H. Dumoulin, E. Riou, B. Jouvin, J.-P. Fénerol, Ph. Palaric, J. Heuving, B. Cartier, and I. Kraus, Physica A **194**, 364 (1993).
[8] I. Kraus, Ph.D. thesis, Orsay, 1995.
[9] J.-C. Geminard, R. Holyst, and P. Oswald, Phys. Rev. Lett. **78**, 1924 (1997). A discussion on the metastability of smectic films using a different approach can be found in Y. Martinez, A. M. Somoza, and L. Mederos, Phys. Rev. E **53**, 2466 (1996).
[10] I. Kraus, P. Pieranski, E. Demikhov, H. Stegemeyer, and J. Goodby, Phys. Rev. E **48**, 1917 (1993).
[11] E. B. Sirota, P. S. Pershan, L. B. Sorensen, and J. Collet, Phys. Rev. A **36**, 2890 (1987); E. B. Sirota, P. S. Pershan, and M. Deutsch, Phys. Rev. A **36**, 2902 (1987).
[12] V. V. Novozhilov, *Thin Shell Theory* (Wolters-Noordhoff, Groningen, 1970).
[13] H. Terrones, J. Phys. Colloq. **51**, C7-347 (1990).
[14] S. Lidin and S. T. Hyde, J. Phys. (Paris) **48**, 1585 (1988).
[15] H. Dumoulin, M. Brazovskaia, and P. Pieranski, Phys. Rev. Lett. **76**, 1655 (1996).
[16] I. Kraus, Ch. Bahr, and P. Pieranski, J. Phys. II **7**, 1617 (1997); Mol. Cryst. Liq. Cryst. **262**, 1 (1995).
[17] M. Ben Amar and P. da Silva, Proc. R. Soc. London, Ser. A (to be published).
[18] M. Eberhardt and R. B. Meyer, Rev. Sci. Instrum. **67**, 2846 (1996); P. Mach, S. Grantz, D. A. Debe, T. Stoebe, and C. C. Huang, J. Phys. II **5**, 217 (1995).